RSC Advances

ROYAL SOCIETY OF CHEMISTRY

www.rsc.org/advances

Graphical Abstract

Nanocomposites constructed by 3D nitrogen-doped graphene (NG) networks with hexagonal $Co(OH)_2$ nanoplates have been prepared via a simple hydrothermal method. The composites are optimized and exhibit a better pseudocapacitive performance than previously reported $Co(OH)_2$ and 2D G/$Co(OH)_2$ composites.

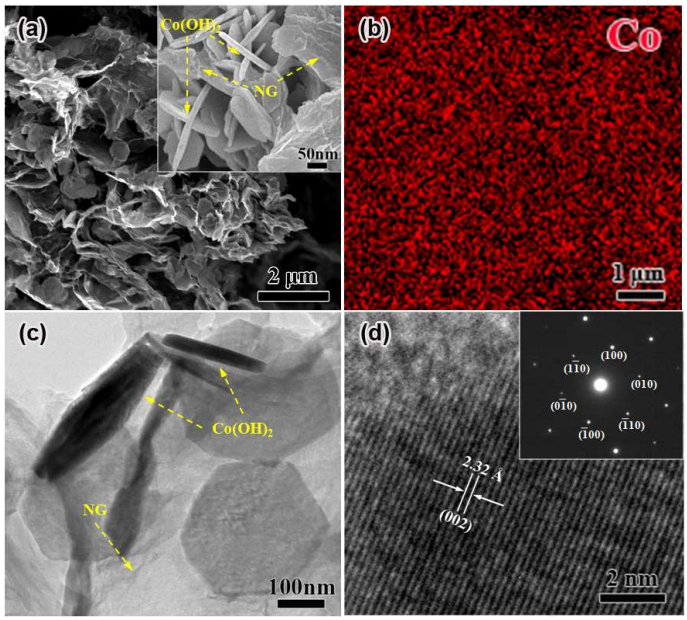

3D Nitrogen-Doped Graphene/$Co(OH)_2$-Nanoplate Composites for High-Performance Electrochemical Pseudocapacitors

Hao Xie‡, Shaochun Tang‡*, Zilun Gong, Sascha Vongehr, Fei Fang, Min Li and Xiangkang Meng*

National Laboratory of Solid State Microstructures, College of Engineering and Applied Sciences, Institute of Materials Engineering, Nanjing University, Jiangsu, People's Republic of China

Abstract

We report a simple hydrothermal synthesis of nanocomposites constructed by 3D nitrogen-doped graphene (NG) networks with hexagonal $Co(OH)_2$ nanoplates which are optimized for application as electrochemical pseudocapacitor material. Single-crystalline $Co(OH)_2$ plates distribute homogeneously inside conductive interconnected NG networks. 71% $Co(OH)_2$ weight content achieves a capacitance of 952 F/g at 1.0 A/g, more than triple that of the pure NG and nearly four times that of $Co(OH)_2$ plates; moreover exceeding the recently reported values for 2D graphene/$Co(OH)_2$ composites. Capacitance retention over 2000 cycles is still high as 95%. The improvements are attributed to the regular morphology of $Co(OH)_2$ and the 3D porosity preventing stacking of $Co(OH)_2$ plates as well as the composite, and the continuously connected pores and highly conductive NG networks facilitating electron and ion transport.

***Keywords*:** Graphene networks, Cobaltous hydroxide, Composites, Supercapacitors

* Corresponding Author: E-mail: tangsc@nju.edu.cn; mengxk@nju.edu.cn.
Tel: (+86) 25 8368 5585; Fax: (+86) 25 8359 5535.

1. Introduction

Developing clean and efficient energy storage is urgent to address the rapidly increasing global energy needs with alternative energy.[1] Supercapacitors are attractive due to their fast charging capability, high power density, and long cycle life.[2,3] Transition metal oxides[4-6] and hydroxides[7-9] are the most promising electrode materials due to their high pseudo-capacitance, low-cost, and environmental compatibility. Among them, $Co(OH)_2$ has a high theoretical capacitance (3460 $F \cdot g^{-1}$), and the practical electrochemical performance depends much on the shape of the material's particles. $Co(OH)_2$ nanostructures with regular shapes such as rods,[10] needles,[11] sheets,[12] and flowers[8] perform better than irregular ones. However, the pseudocapacitors based on such materials rely on faradic redox reactions, and the active electrode materials are typically too insulating to support the fast electron transport required by high charging rates.[13] An enhancement of performances via a combination with conductive materials is thus highly desired.

Graphene (G) is a flexible single-atom layer with large specific surface area and high electrical conductivity.[14-15] It is a promising supercapacitor electrode material, and demonstrated to be an ideal matrix for functional nanomaterials to improve electrochemical performance.[16,17] For example, G/MnO_2 composite exhibits high capacitance even at fast charging rates and an energy density of 51 Wh/kg.[18] 2D $G/Co(OH)_2$ with a specific capacitance of 972.5 F/g at 0.5 A/g was prepared by one-step refluxing.[19] A simple and rapid one-pot process for synthesizing reduced graphene oxide/$Co(OH)_2$ led also to enhanced electrochemical properties for

supercapacitors.[20] G/$Co(OH)_2$ as a high performance anode material for lithium batteries was prepared through a one-step hydrothermal method.[21] Little work, however, has focused on composite nanostructures with regularly shaped $Co(OH)_2$. $Co(OH)_2$ and $Ni(OH)_2$ nanoplates on G-sheets exhibit 436 F/g[22] and 953 F/g[23] respectively even at high current densities around 50 A/g and while retaining excellent cycling behaviours. Stacking of such 2D structures lowers the specific surface area. Although the 2D G/$Co(OH)_2$ composites avoid the stacking of $Co(OH)_2$ nanoplates and thus show superior electrochemical performance, all these products are mainly still 2D graphene, therefore the stacking of the composite is not avoided. Macroscopic G networks have their nanosheets folded into 3D architectures with high specific surface area, suitable nano- or micropores and network-like connection.[24,25] The sheets do not stack but still connect with each other, resulting in a conducting network for fast, multi-dimensional electron transport between the active materials and the charge collector, as well as ion transport through the pore network.[26,27] In addition, nitrogen-doping enhances the electrochemical properties of graphene-based electrode materials significantly because an incorporation of the heteroatom N can improve electronic conductivity.[28-30]

Here, an advanced integrated composite material is designed by combining 3D N-doped graphene (NG) with hexagonal $Co(OH)_2$ nanoplates, and synthesized via a simple hydrothermal method. Developing the procedure involved optimizing parameters like graphene oxide (GO) precursor concentration and $Co(OH)_2$ content, which were independently optimized while aiming for high porosity and high capacity,

respectively. The $Co(OH)_2$ rather stands randomly in the 3D networks than lies on NG sheets, further increasing specific surface area. Thus, these NG/$Co(OH)_2$ composites exhibit a better pseudocapacitive performance than previously reported $Co(OH)_2$ and 2D G/$Co(OH)_2$ composites. The capacitance retention is still 95% after 2000 cycles.

2. Experimental section

2.1 Synthesis of NG/$Co(OH)_2$ composites

In the typical synthesis, a solution containing 0.04 M $CoCl_2 \cdot 6H_2O$, 0.2 M $C_6H_5Na_3O_7 \cdot 2H_2O$, 0.15 M $NaH_2PO_4 \cdot H_2O$, and 0.2 M NaOH was prepared by dissolving them one after another into 100 ml deionized water. The purple mixture was stirred in a 50 ^oC water bath for 30 min. 10 ml of the resulting grey solution was added into 40 ml of 2 mg/ml GO suspension, which can be synthesized by a modified Hummers method as described in the Electronic Supplementary Information. 500 μl ethylenediamine was added under magnetic stir for 15 min. The mixture was transferred to a 100 ml Teflon-lined autoclave. Hydrothermal reaction at 160 ℃ proceeded for 12 h. The products were purified by centrifugation from deionized water and dried in a freeze dryer for 7 h. For comparison, pure 3D porous GN networks and $Co(OH)_2$ nanoplates were also prepared by almost the same procedure absent the undesired chemicals, i.e. the synthesis of NG used 50 ml of GO suspension.

2.2 Characterizations

The products were characterized by X-ray diffraction (XRD) with a D/Max-RA X-ray diffractometer (Cu Kα =1.5418 Å radiation) at 2^o/min. The elements' valence

states were examined by X-ray photoelectron spectroscopy (XPS) in a Thermo VG Scientific MultiLab ESCA2000 system with a CLAM4 hemispherical analyzer at a base pressure below 3×10^{-10} mbar. The morphology and sizes of the products were analyzed by field-emission scanning electron microscopy (FE-SEM) on S-4800 (Hitachi) at 10 kV, and transmission electron microscopy (TEM), and selected area electron diffraction (SAED) on a JEM-2100 (JEOL) at an acceleration voltage of 200 kV. Energy dispersed X-ray spectroscopy (EDS) was performed on the same FE-SEM microscope. Fourier transform infrared (FTIR) spectra of KBr powder pressed pellets were recorded with a Varian 3100 FTIR spectrometer. Thermogravimetric analysis (TGA) was performed on a TGA/SDTA thermogravimetric analyzer from room temperature (r.t.) to 800°C in air at a heating rate of 20 ^{o}C/min.

2.3 Electrochemical measurements

The working electrodes were prepared by grinding the active materials, acetylene black and polytetrafluoroethylene (mass ratio 7:2:1). Then, the mixture was rolled into film and pressed with 10 MPa onto the Ni foam. The effective area of a working electrode is 1 cm^2 and the mass loading of active material is about 2 mg. The measurements were done at room temperature on a Metrohm Autolab 302N electrochemical workstation in a three-electrode system with a platinum foil counter electrode and an Ag/AgCl reference. The used electrolyte was 6 M KOH. Cyclic voltammetry (CV) scans were recorded from 0 to 0.5 V (vs. Ag/AgCl) at various scan rates. Specific capacitance was established via the integral under the CV curve calculated by the software using the formula $SC = \int i\, dV/(2vm\Delta V)$, where v is the scan

rate, m the mass of the active material, and ΔV is the operating potential range. Galvanostatic charge-discharge (CD) cycle tests were carried out in the range of 0~0.3 V at various current densities. Capacitance retention was tested on a Land Battery Test System (Wuhan Kingnuo Electronic Company, China). The anode is the same as the above described working electrode, and the cathode is blank nickel foam. The current density and potential windows are the same as those in the galvanostatic measurements. The capacitance retention of a cycle equals its discharge time divided by the discharge time of the first cycle. In the electrical impedance spectroscopy (EIS) measurements, AC amplitude was 5 mV, frequency ranges from 10^5 to 0.1 Hz.

3. Results and discussion

In order to obtain 3D NG networks, the concentration of GO suspension in the reactions from GO to NG was optimized to be the recommended value (2 mg/ml). The pure NG network is continuously connected (Figure S1a). During hydrothermal synthesis of NG/$Co(OH)_2$ composites, mixed solutions containing chemicals necessary for both the $Co(OH)_2$ nanoplates and the NG were used. Figure 1a shows an SEM image of the NG/$Co(OH)_2$ obtained from a typical synthesis. The resulting 3D NG network in the NG/$Co(OH)_2$ composite is not changed too much. The composite has a 3D porous structure with the NG also continuously connected. From the higher magnification (inset of Figure 1a) of a particularly dense region of $Co(OH)_2$ nanoplates one can see that they do not stack, but their presence makes a finer porous structure. Compared to pure $Co(OH)_2$ nano plates (Figure S1b-d), the plates in the composite remain the hexagonal morphology and their stacking is avoided. The

hexagons' edge lengths are roughly 175 nm. They are about 10~15 nm thick. EDS elemental mapping of Co (Figure 1b) reveals that the hexagons are homogeneously distributed throughout the composite. TEM image (Figure 1c) confirms that the plates are well-dispersed and randomly distributed. The lattice fringes visible in the HRTEM image (Figure 1d) recorded from an edge of an individual $Co(OH)_2$ plate show that it is a single crystal. The inter-planar distance is measured to be 2.32 Å, which corresponds to the (002) planes of $Co(OH)_2$. The SAED pattern (the inset) recorded from a single plate confirms its single-crystalline nature.

Figure 2 shows XRD patterns of pure NG (black curve), $Co(OH)_2$ (magenta curve), and the NG/$Co(OH)_2$ composites with $Co(OH)_2$ contents of 54.5 wt% and 92.6 wt.%. In the XRD pattern (blue curve) of the typical NG/$Co(OH)_2$ composite, most of the diffraction peaks correspond to the crystal planes of brucite-like $Co(OH)_2$ (JCPDS 30-0443). A broad and weak diffraction (marked by a green dashed circle) is observed at about 26.4° and assigned to be the (002) of graphene. The inter-layer spacing is calculated to be 3.42 Å, which is much lower than that of the precursor GO (8.02 Å), but slightly higher than natural graphite (3.37Å).[31] A characteristic GO peak at 11.03° (Figure S2a) is not visible, indicating complete conversion to graphene. No peaks from other phases are present. With increasing the $Co(OH)_2$ content, the graphene signal in XRD patterns weakens while $Co(OH)_2$ peaks become stronger. The peak of graphene is not clearly identified at a high content of 92.6 wt.%, which is due to that the graphene signals are masked by the $Co(OH)_2$. FTIR spectra (Figures S2b and S3) and XPS analysis (Figure S4) prove the presence of $Co(OH)_2$, doping of N

into the carbon matrix, as well as confirming complete conversion of GO, which are all discussed in detail in the Electronic Supplementary Information.

TGA analysis was used in order to determine the $Co(OH)_2$ content in the composites, which is controlled via the Co^{2+} concentration. The TGA curve (Figure 3) of the typical composite shows an initial mass loss (stage I) due to evaporation of water. The mass loss in stage II from 180 ^oC to the inflection point at 300 ^oC results from the dehydration of $Co(OH)_2$ into Co_3O_4.[32] The subsequent loss until 450 ^oC (stage III) results from the combustion of NG.[22] The $Co(OH)_2$ content in this composite is thus calculated to be 71.3 wt.% of the dry NG/$Co(OH)_2$ product (after stage I), namely according to the stage II loss, which is consistent with that based on the finally remaining Co_3O_4.

Electrochemical performance of the NG/$Co(OH)_2$ composites is highly dependent on the $Co(OH)_2$ content. Figure 4 shows average capacitances of NG/$Co(OH)_2$ composites with different $Co(OH)_2$ contents, including 0 wt.% (pure NG), low, optimal, high, and 100 wt.% being for a sample of pure hexagonal nano plates, all measured at various discharge current densities (nine samples with different contents were investigated). Also, the electrochemical performance of a physical mixture of NG and $Co(OH)_2$ with 54.5 wt.% $Co(OH)_2$ was measured. The capacitance values of the NG/$Co(OH)_2$ are all higher than those of pure NG, $Co(OH)_2$ nanoplates and their physical mixture. The capacitances all decrease similarly with the current density; the especially initially slightly lower slope at low $Co(OH)_2$ contents may indicate the higher electrical conductivity due to NG. At the same $Co(OH)_2$

percentage of 54.5 wt%, the specific capacitances of the NG/$Co(OH)_2$ are all about 1.5 times higher than those of the mixture (comparing black curve with dark yellow one). At current densities higher than 4 A/g, the decreasing rate of the physical mixture's capacitance with an increase of current density is faster than that of the NG/$Co(OH)_2$. This is because a simple physical mixing leads to a stacking of plates. The capacitance is maximal for 71.3 wt.% $Co(OH)_2$. Below that value, the content of active $Co(OH)_2$ is not optimized; above that value, the $Co(OH)_2$ plates become too numerous and start to stack together again, leading to a decreased electrochemical activity. The capacitance of the optimal NG/$Co(OH)_2$ composite reaches 952.4 F/g at a current density of 1.0 A/g, which is nearly four times that of bare $Co(OH)_2$ nanoplates (250.0 F/g) and NG networks (283.3 F/g). It exceeds the recently reported values of 474 F/g[20] and 642.5 F/g[33] (all at 1.0 A/g) for reduced graphene oxide/$Co(OH)_2$ and $Co(OH)_2$-nanowires/graphite composites, respectively. At 2.0 A/g, the specific capacitance of our NG/$Co(OH)_2$ is 847.5 F/g, which is higher than those of the $Co(OH)_2$/2D graphene sheet-on-sheet hybrid (622 F/g)[22] and the $Co(OH)_2$ nanoflakes grown on ultrastable Y zeolite (650 F/g).[34] Also, it is higher than that of $Co(OH)_2$/graphene/Ni foam (693.8 F/g) synthesized by radio-frequency plasma enhanced chemical vapor deposition.[35] The superior performances may be due to the regular morphology of $Co(OH)_2$ particles, N-doping of G, and the 3D porosity preventing stacking of $Co(OH)_2$ plates and the composite, as well as the optimized accessible large specific surface area and the hierarchical composite architecture. The capacity is still 686.2 F/g at ten times the current density, a high 72% capacitance

retention. The continuously connected pores and highly conductive NG networks facilitating electron and ion transport.[36] Also, a synergistic effect between different components of NG and $Co(OH)_2$ plays a key role.

The synergistic effect between NG and $Co(OH)_2$ is suggested as follows: (1) Both NG and $Co(OH)_2$ are positive pseudo-capacitance materials,[8,28-30] and can contribute the capacitances of the hydrothermally synthesized NG/$Co(OH)_2$ composites. The synergistic effect improves the capacitance higher than each of them. (2) Combining NG and $Co(OH)_2$ into composites during a hydrothermal reaction significantly improves the supercapacitive performance, which cannot be achieved by physical mixing or adjusting morphology and structure of pure NG and $Co(OH)_2$. The synergy is similar to that in the hybrids of graphene and metal hydroxides.[22,23] (3) The specific capacitance of NG/$Co(OH)_2$ does not increase monotonously, but is optimized to be maximal at a $Co(OH)_2$ percentage of 71.3 wt.%. This indicates that the electrochemical performance of the NG/$Co(OH)_2$ composites is highly composition-dependent, and is a reflection about the synergistic effect between them.

Figure 5a shows CV curves of the optimal NG/$Co(OH)_2$ composite at scan rates from 5 to 100 mV/s. The redox current peaks are attributed to the reversible reaction $Co^{2+} \leftrightarrow Co^{4+}$, which results in a pseudocapacitive shape.[37] Figure 5b shows the corresponding specific capacitance values. The capacitance is still 475.6 F/g even at a high scan rate of 100 mV/s, which is 64% of the capacity at 5 mV/s (740.4 F/g). Improved rate performance can be attributed to that a high specific surface area is favorable for fast migration of OH^- ions in the electrolyte to the surface of both

$Co(OH)_2$ sheets and NG. Figure 5c shows the CD characteristics in a potential range of 0~0.4 V at various specific current densities. The curves' shape indicates that the materials have a reversible charge/discharge capacitance. The galvanostatic discharge time at 1.0 A/g is up to 90 seconds indicating a high capacitance, which is consistent with the CV results. To further understand the electrochemical performance characteristics, EIS of the optimal NG/$Co(OH)_2$ composite was analyzed by using Nyquist plots. Figure 5d shows EIS of pure NG, $Co(OH)_2$, and NG/$Co(OH)_2$ composites with $Co(OH)_2$ contents of 54.5, 71.3 and 92.6 wt.%. Obviously, the EIS plot contains a partially overlapped semicircle and a straight sloping line. The semicircle at high frequencies is associated with Faradic charge-transfer resistance. The almost vertical line in the low frequency region is indicative of the rapid ion transport that the porosity allows between electrode and electrolyte as well as through the latter.[38] Through a fitting analysis of the Nyquist plot, the related R_{ct} (see inset equivalent circuit) of the optimal NG/$Co(OH)_2$ composite has the lowest value of 1.2 Ω. W is the Warburg impedance (the slope of the curves at a low frequency), and R_b is bulk resistance of the electrochemical system, indicating the conductivity of the electrolyte and internal resistance of the electrode. R_b values are determined by the point where the semicircle intersects with the Z' axis. The R_b values of pure NG, $Co(OH)_2$, 54.5 wt%, 71.3 wt%, and 92.6 wt% composites are 0.5 Ω, 0.8 Ω, 0.38 Ω, 0.42 Ω and 0.59 Ω, respectively. The optimal NG/$Co(OH)_2$ composite has the lowest R_b value, which is consistent with that of specific capacitances. The low values of R_b

and R_{ct} is because graphene is cross-linked by N to form a 3D networks with an excellent conductivity and the structure design prevents the staking of NG and plates.

The cycling stability was evaluated by repeating the CD test. Figure 6 shows the capacitance retention for 2000 cycles at a current density of 1.0 A/g. The inset shows the cycles from 1990 to 2000, revealing a very regular timing. The specific capacitance of the NG/$Co(OH)_2$ electrode stays at 95% of the initial specific capacitance, proving stable electrochemical properties in the range of 0~0.3 V.

4. Conclusions

A novel 3D N-doped porous graphene network supporting hexagonal $Co(OH)_2$ nanoplates is prepared by a simple hydrothermal synthesis. The plates distribute homogeneously, and such structure prevents the staking of the nanoplates and GN. The novel composite exhibits a capacitive performance far better than the pure 3D GN or $Co(OH)_2$ alone. After optimizing the $Co(OH)_2$ content, the new composites show higher specific capacitances than the recently reported values for 2D graphene/$Co(OH)_2$ composites, even at fast charging rates. The NG/$Co(OH)_2$ composites exhibit excellent capacitance retention of 95% over 2000 cycles. The superior performance is due to the regular morphology of $Co(OH)_2$, the 3D porosity preventing stacking of $Co(OH)_2$ plates, as well as the hierarchical architecture and highly conductive NG networks facilitate electron and ion transport.

Electronic supplementary information (ESI) available

Experimental details for synthesis of GO suspensions, SEM and TEM images of NG and $Co(OH)_2$, XRD patterns of G, GO and NG, FTIR and XPS spectra of NG, GO $Co(OH)_2$, and the NG/$Co(OH)_2$ composites.

Notes

The authors declare no competing financial interest.

‡ Hao Xie and Shaochun Tang contributed equally to this work.

Acknowledgments

The authors kindly acknowledge the joint support by the PAPD, the Fundamental Research Funds for the Central Universities, the National Natural Science Foundation of Jiangsu Province, the National Natural Science Foundation of China and the State Key Program for Basic Research of China.

References

1 S. W. Lee, N. Yabuuchi, B. M. Gallant, S. Chen, B. S. Kim, P. T. Hammond and Y. Shao-Horn, *Nat. Nanotechnol.*, 2010, **5**, 531-537.

2 P. Simon and Y. Gogotsi, *Nat. Mater.*, 2008, **7**, 845-854.

3 J. R. Miller and P. Simon, *Science*, 2008, **321**, 651-652.

4 X. Xia, J. Tu, Y. Zhang, X. Wang, C. Gu, X. B. Zhao and H. J. Fan, *ACS Nano*,

2012, **6**, 5531-5538.

5 Y. M. Dai, S. C. Tang, S. Vongehr and X. K. Meng, *ACS Sustainable Chem. Eng.*, 2014, **2**, 692-698.

6 Y. Q. Zhang, X. H. Xia, J. P. Tu, Y. J. Mai, S. J. Shi, X. L. Wang and C. D. Gu, *J. Power Sources*, 2012, **199**, 413-417.

7 V. Gupta, T. Kusahara, H. Toyama, S. Gupta and N. Miura, *Electrochem. Commun.*, 2007, **9**, 2315-2319.

8 S. C. Tang, S. Vongehr, Y. G. Wang, L. Chen and X. K. Meng, *J. Solid State Chem.*, 2010, **183**, 2166-2173.

9 Y. Shen, J. Yin, F. Gao, J. Wang, H. Pang and Q. Lu, *Chem. Commun.*, 2010, **46**, 6183-6185.

10 J. T. Sampanthar and H. C. Zeng, *J. Am. Chem. Soc.*, 2002, **124**, 6668-6675.

11 L. Q. Zhang, A. K. Dutta, G. Jarero and P. Stroeve, *Langmuir*, 2000, **16**, 7095-7100.

12 E. Hosono, S. Fujihara and I. Honma, *J. Mater. Chem.*, 2005, **15**, 1938-1945.

13 Y. M. Dai, S. C. Tang, J. Q. Peng, H. Y. Chen, Z. X. Ba, Y. J. Ma and X. K. Meng, *Mater. Lett.*, 2014, **130**, 107-110.

14 D. Wang, D. Choi, J. Li, Z. Yang, Z. Nie, R. Kou, D. Hu, C. Wang, L. V. Saraf, J. Zhang, I. A. Aksay and J. Liu, *ACS Nano*, 2009, **3**, 907-914.

15 K. Zhang, L. L. Zhang, X. S. Zhao and J. Wu, *Chem. Mater.*, 2010, **22**, 1392-1401.

16 J. X. Zhu, T. Zhu, X. Z. Zhou, Y. Y. Zhang, X. W. Lou, X. D. Chen, H. Zhang, H.

H. Hng and Q. Y. Yan, *Nanoscale*, 2011, **3**, 1084-1089.

17 Z. S. Wu, W. C. Ren, L. Wen, L. B. Gao, J. P. Zhao, Z. P. Chen, G. M. Zhou, F. Li and H. M. Cheng, *ACS Nano*, 2010, **4**, 3187-3194.

18 Z. Fan, J. Yan, T. Wei, L. Zhi, G. Ning, T. Li and F. Wei, *Adv. Funct. Mater.*, 2011, **21**, 2366-2375.

19 S. Chen, J. W. Zhu and X. Wang, *J. Phys. Chem. C*, 2010, **114**, 11829-11834.

20 Z. P. Li, J. Q. Wang, L. Y. Niu, J. F. Sun, P. W. Gong, W. Hong, L. M. Ma and S. G. Yang, *J. Power Sources*, 2014, **245**, 224-231.

21 Y. S. He, D. W. Bai, X. W. Yang, J. Chen, X. Z. Liao and Z. F. Ma, *Electrochem. Commun.*, 2010, **12**, 570-573.

22 C. Y. Sun, Y. G. Zhu, T. J. Zhu, J. Xie, G. S. Cao and X. B. Zhao, *J. Solid State Electrochem.*, 2013, **17**, 1159-1165.

23 H. Wang, H. S. Casalongue, Y. Liang and H. Dai, *J. Am. Chem. Soc.*, 2010, **132**, 7472-7477.

24 X. H. Cao, Z. Y. Yin and H. Zhang, *Energy Environ. Sci.*, 2014, **7**, 1850-1865.

25 Y. N. Meng, Y. Zhao, C. G. Hu, H. H. Cheng, Y. Hu, Z. P. Zhang, G. Q. Shi and L. T. Qu, *Adv. Mater.*, 2013, **25**, 2326-2331.

26 J. S. Lee, S. I. Kim, J. C. Yoon and J. H. Jang, *ACS Nano*, 2013, **7**, 6047-6055.

27 Z. Niu, J. Chen, H. H. Hng, J. Ma and X. Chen, *Adv. Mater.*, 2012, **24**, 4144-4150.

28 D. W. Wang, Y. G. Min, Y. H. Yu and B. Peng, *J. Colloid Interface Sci.*, 2014, **417**, 270-277.

29 C. D. Wang, Y. G. Zhou, L. F. He, T. Ng, G. Hong, Q. H. Wu, F. Gao, C. S. Lee and W. J. Zhang, *Nanoscale*, 2013, **5**, 600-605.

30 T. Wang, L. X. Wang, D. L. Wu, W. Xia, H. Y. Zhao and D. Z. Jia, *J. Mater. Chem. A*, 2014, **2**, 8352-8361.

31 D. S. Genga, S. L. Yang, Y. Zhang, J. L. Yang, J. Liu, R. Y. Li, T. K. Sham, X. L. Sun, S. Y. Ye and S. N. Knights, *Appl. Surf. Sci.*, 2011, **257**, 9193-919.

32 C. Nethravathi, C. R. Rajamathi, M. Rajamathi, X. Wang, U. K. Gautam, D. Golberg and Y. Bando, *ACS Nano*, 2014, **8**, 2755-2765.

33 J. Jiang, J. P. Liu, R. M. Ding, J. H. Zhu, Y. Y Li, A. Z. Hu, X. Li and X. T. Huang, *ACS Appl. Mater. Interfaces*, 2011, **3**, 99-103.

34 Y. Y. Liang, L. Cao, L. B. Kong and H. L. Li, *J. Power Sources*, 2004, **136**, 197-200.

35 C. M. Zhao, X. Wang, S. M. Wang, Y. Y. Wang, Y. X. Zhao and W. T. Zheng, *Int. J. Hydrogen Energy*, 2012, **37**, 11846-11852.

36 L. L. Jiang and Z. J. Fan, *Nanoscale*, 2014, **6**, 1922-1945.

37 Z. P. Li, J. Q. Wang, L. Y. Niu, J. F. Sun, P. W. Gong, W. Hong, L. M. Ma and S. G. Yang, *J. Power Sources*, 2014, **245**, 224-231.

38 L. Wan, J. W. Xiao, F. Xiao and S. Wang, *ACS Appl. Mater. Interfaces*, 2014, **6**, 7735-7742.

Figures and captions

Figure 1. (a) SEM, (b) EDS-mapping of Co, and (c) TEM images of the typical NG/$Co(OH)_2$ composite, and (d) a HRTEM of $Co(OH)_2$ hexagons. The inset of (a) magnifies a particularly dense accumulation of nanoplates in the 3D NG; and the inset of (d) is a SAED pattern recorded from a hexagon.

Figure 2. XRD patterns of pure NG (black curve), $Co(OH)_2$ (magenta curve), and the NG/$Co(OH)_2$ composites with different $Co(OH)_2$ contents.

Figure 3. TGA curve of the typical NG/$Co(OH)_2$ composite recorded from room temperature to 800 ^oC.

Figure 4. Specific capacitances of NG/$Co(OH)_2$ composites with different $Co(OH)_2$ contents at various charge-discharge current densities. A physical mixture of NG and $Co(OH)_2$ with 54.5 wt% $Co(OH)_2$ is also provided for comparison.

Figure 5. (a) CV curves of the optimal NG/$Co(OH)_2$ composite with 71.3 wt.% $Co(OH)_2$ at various scan rates, and (b) corresponding average specific capacitances, (c) galvanostatic charge-discharge curves at various current densities, and (d) EIS curves of pure NG, $Co(OH)_2$, and NG/$Co(OH)_2$ composites with different $Co(OH)_2$ contents. Insets in (d) are the equivalent circuit and a magnified EIS.

Figure 6. Capacitance retention of the optimal NG/$Co(OH)_2$ composite at 1.0 A/g over first 2,000 cycles. The inset shows galvanostatic charge and discharge curves from 1990 to 2000 cycles.

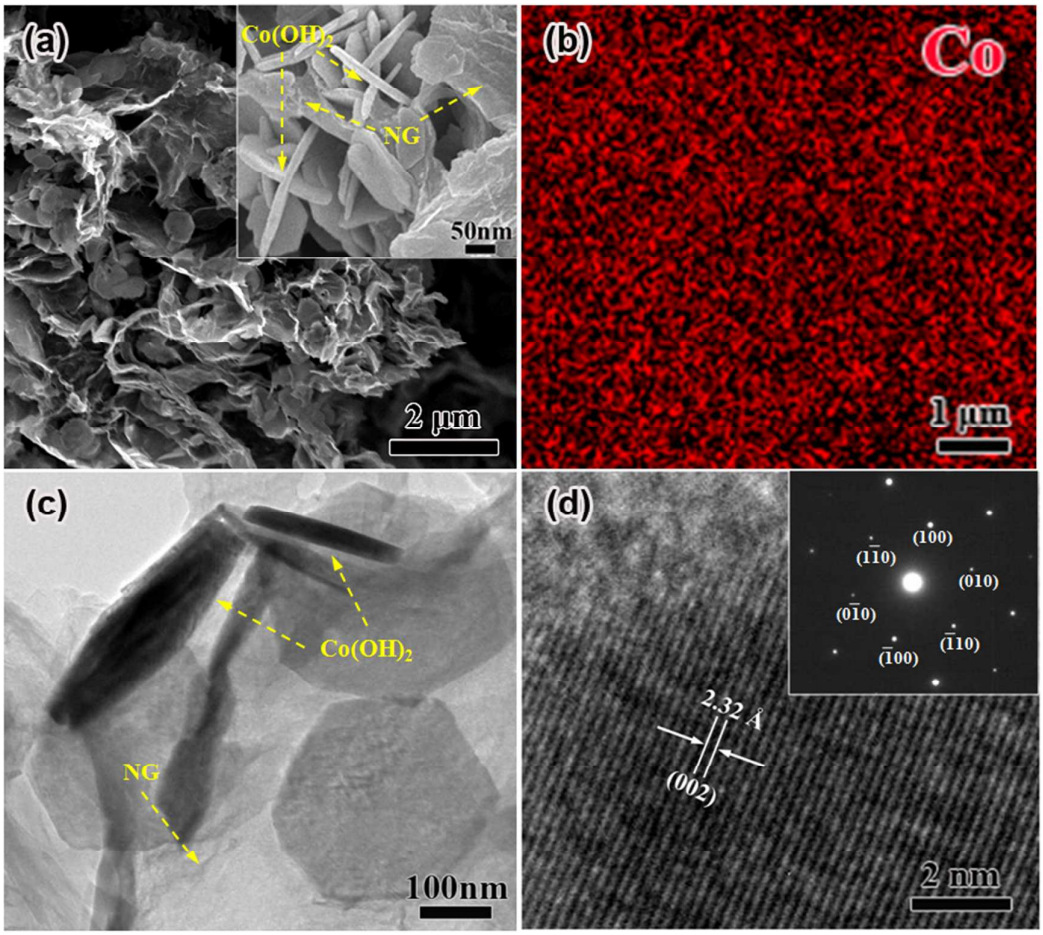

Figure 1. (a) SEM, (b) EDS-mapping of Co, and (c) TEM images of the typical NG/$Co(OH)_2$ composite, and (d) a HRTEM of $Co(OH)_2$ hexagons. The inset of (a) magnifies a particularly dense accumulation of nanoplates in the 3D NG; and the inset of (d) is a SAED pattern recorded from a hexagon.

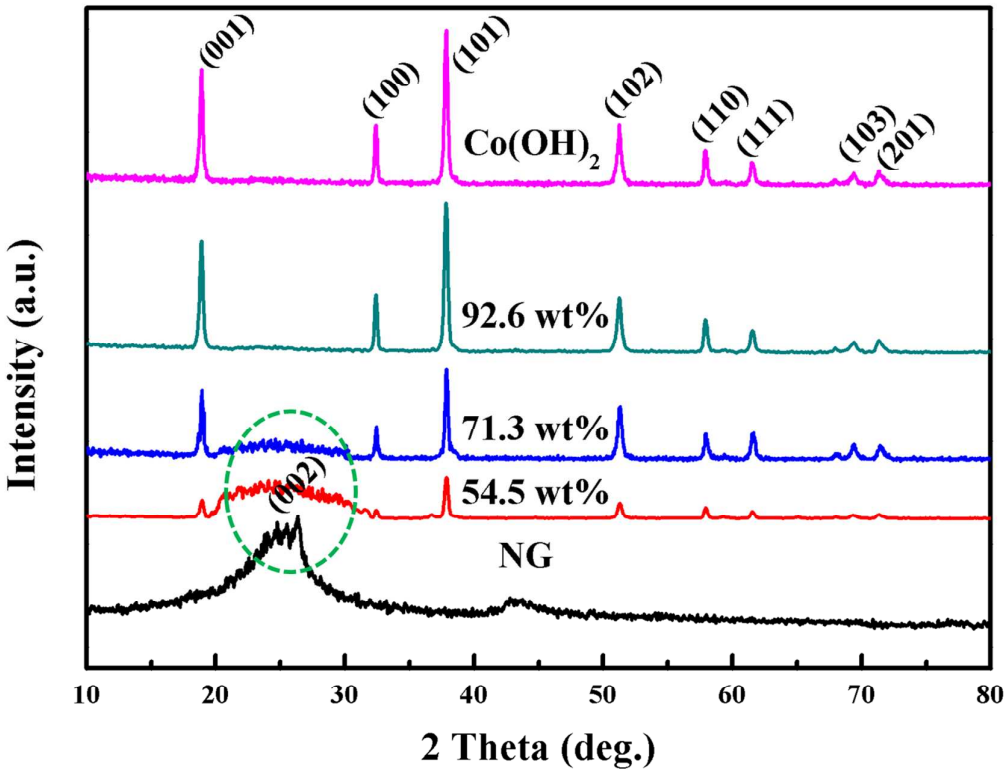

Figure 2. XRD patterns of pure NG (black curve), $Co(OH)_2$ (magenta curve), and the NG/$Co(OH)_2$ composites with different $Co(OH)_2$ contents.

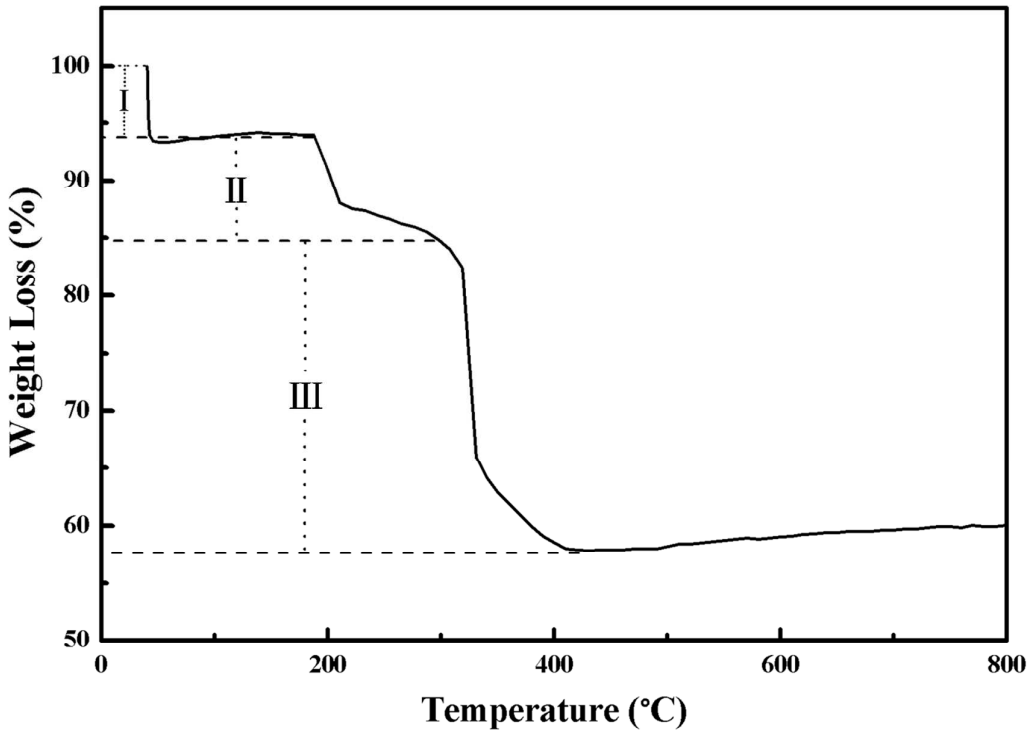

Figure 3. TGA curve of the typical NG/$Co(OH)_2$ composite recorded from room temperature to 800 ^{o}C.

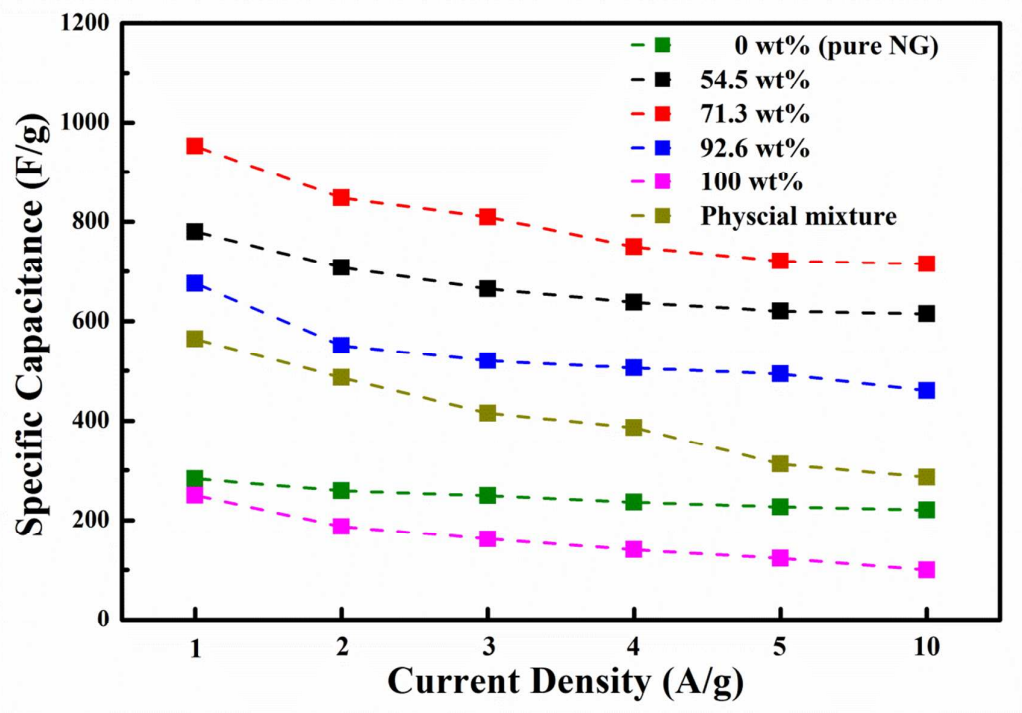

Figure 4. Specific capacitances of NG/$Co(OH)_2$ composites with different $Co(OH)_2$ contents at various charge-discharge current densities. A physical mixture of NG and $Co(OH)_2$ with 54.5 wt% $Co(OH)_2$ is also provided for comparison.

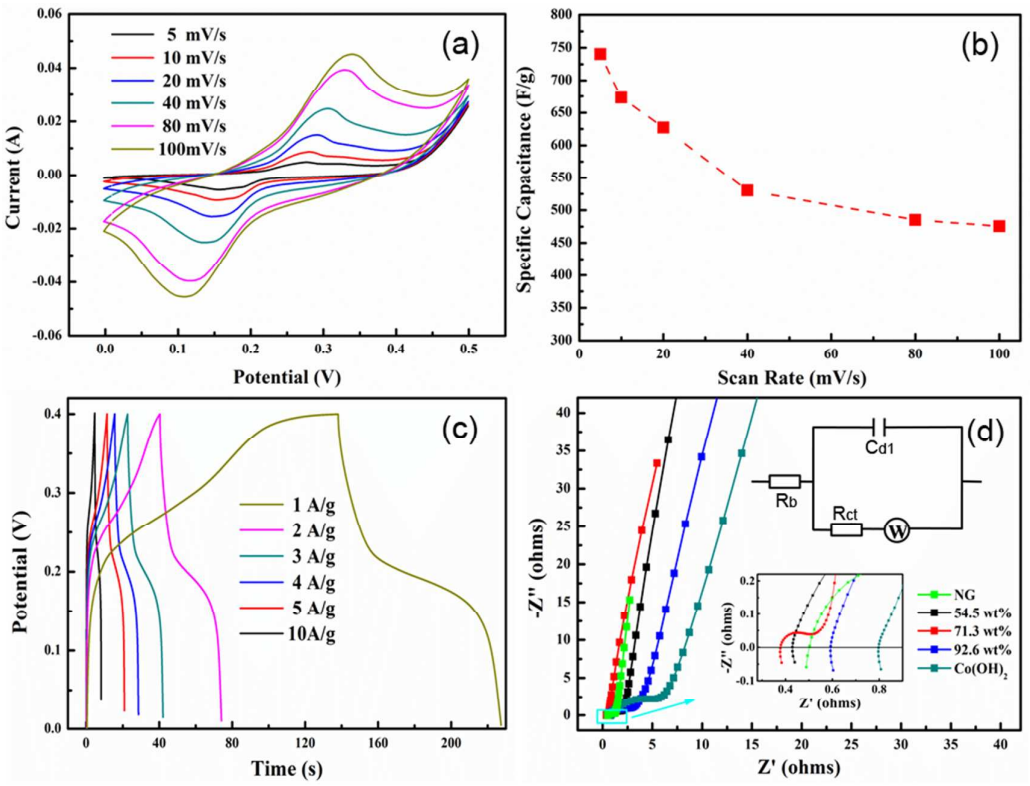

Figure 5. (a) CV curves of the optimal NG/$Co(OH)_2$ composite with 71.3 wt.% $Co(OH)_2$ at various scan rates, and (b) corresponding average specific capacitances, (c) galvanostatic charge-discharge curves at various current densities, and (d) EIS curves of pure NG, $Co(OH)_2$, and NG/$Co(OH)_2$ composites with different $Co(OH)_2$ contents. Insets in (d) are the equivalent circuit and a magnified EIS.

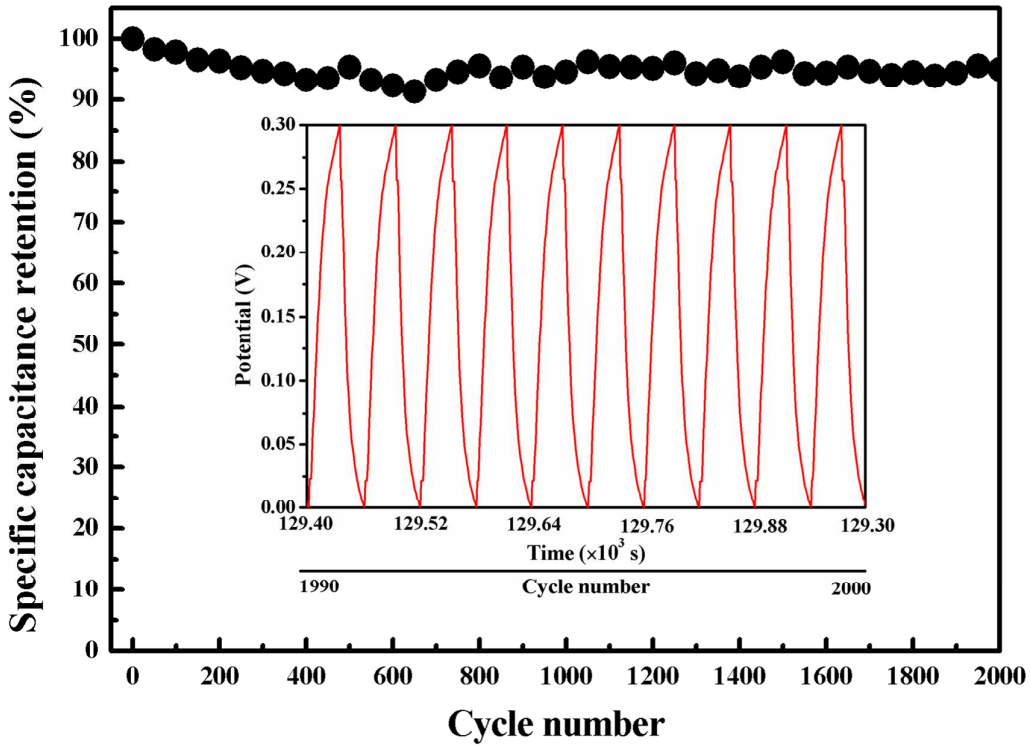

Figure 6. Capacitance retention of the optimal NG/$Co(OH)_2$ composite at 1.0 A/g over first 2,000 cycles. The inset shows galvanostatic charge and discharge curves from 1990 to 2000 cycles.